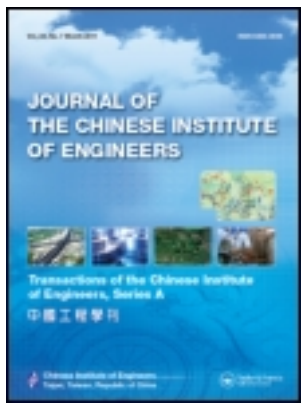

Journal of the Chinese Institute of Engineers
Publication details, including instructions for authors and subscription information:
http://www.tandfonline.com/loi/tcie20

Evaporation of water film in an enclosure filled with a porous medium

Wu-Shung Fu [a] & Wen-Wang Ke [a]
[a] Department of Mechanical Engineering , National Chiao Tung University , 1001 Ta Hsueh Road, Hsinchu, 30050, Taiwan, Republic of China
Published online: 03 Mar 2011.

To cite this article: Wu-Shung Fu & Wen-Wang Ke (1999) Evaporation of water film in an enclosure filled with a porous medium, Journal of the Chinese Institute of Engineers, 22:3, 325-339, DOI: 10.1080/02533839.1999.9670470

To link to this article: http://dx.doi.org/10.1080/02533839.1999.9670470

Journal of the Chinese Institute of Engineers, Vol. 22, No. 3, pp. 325-339 (1999)

EVAPORATION OF WATER FILM IN AN ENCLOSURE FILLED WITH A POROUS MEDIUM

Wu-Shung Fu* and Wen-Wang Ke
Department of Mechanical Engineering
National Chiao Tung University
1001 Ta Hsueh Road, Hsinchu, 30050, Taiwan
Republic of China

Key Words: evaporation, porous medium, latent heat, sensible heat.

ABSTRACT

A double diffusive natural convection in an enclosure filled with a porous medium is investigated numerically. To enhance the heat transfer rate of a heat wall, the heat wall is wetted with a thin water film, then sensible and latent heat transfer occur simultaneously. The Darcy-Brinkman-Forchheimer model is used and the factors of heat flux, porosity and diameter of bead are taken into consideration. The SIMPLEC method with iterative processes is adopted to solve the governing equations. The results show that the effect of evaporation on the heat transfer rate is apparent, and the latent heat transfer plays an important role in the high Darcy-Rayleigh number situations. The averaged Nusselt number $\overline{Nu}$ is approximately 2.5 when $Ra^*<4$. In the range of $4<Ra^*<4469$, the relationship of the averaged Nusselt number with the Darcy-Rayleigh number is linear in logarithmic scale.

I. INTRODUCTION

Double diffusive natural convection in a porous medium has many important applications in energy-related engineering problems, such as moisture migration in fibrous insulation, diffusion of pollutants in saturated soil, and flow in the wick of a heat pipe. Although numerous investigations have studied the problem of double diffusive natural convection in a porous medium numerically and experimentally, due to the complexity of temperature and flow fields in the porous medium, the subject has continued to be a focus of research in the last decade.

Trevisan and Bejan (1985) investigated the effects of heat and mass transfer on natural convection in a porous medium by numerical simulations and scale analysis. The results of the scale analysis were in agreement with those produced by the discrete numerical experiments, and sorted out many effects which influence overall heat and mass transfer results of numerical experiments. Lai and Kulacki (1991) studied a vertical plate embedded in a saturated porous medium and utilized a similar method to solve governing equations derived from Darcy's law and Boussinesq approximation. The results showed that the effect of the Lewis number on the concentration convection field was more pronounced than that of the temperature and flow fields. Hsiao *et al.* (1992) conducted a numerical investigation of natural convection of a heated horizontal cylinder in an enclosure filled with a porous medium. The results pointed out that the effect of thermal dispersion on the natural convection was small from ranging from low to moderate Rayleigh numbers, and the numerical solutions were in better agreement with the experimental data. Alavyoon (1993) also used a numerical method

*Correspondence addressee

to study unsteady and steady convection in a fluid-saturated vertical and homogenous porous medium. The results indicated that as the Lewis number was larger than 1, there existed a minimum aspect ratio below which the concentration field in the core region was rather uniform and above which it was linearly stratified in the vertical direction. Alavyoon *et al.* (1994) subsequently studied the above subject with opposite and horizontal gradients of heat and solute conditions. The results revealed that under a certain domain the convection oscillated and outside this domain the convection approached a steady state. Nithiarasu *et al.* (1997) studied a generalized non-Darian porous medium model with constant and variable porosities for natural convective flow. The results indicated the wall Nusselt number was significantly affected by the combination of Rayleigh number, Darcy number and porosity in the non-Darcy flow regime, and the model was able to predict the channeling effect. Murray and Chen (1989) carried out an experimental study to examine double-diffusive convection in a porous medium, and the results showed that as the temperature difference was reduced from supercritical to subcritical values, the heat flux curve established a hysteresis loop. Lauriat and Prasad (1989) investigated non-Darcian effects on natural convection in a vertical porous enclosure, and the results showed that the effect of Prandtl number on Nussult number was not straight forward and depended on the flow regime and other parameters.

Because of the difficulties associated with the theoretical determination of effective thermal conductivity for the corresponding porous medium situation, a number of experimental studies investigating the effective thermal conductivity were conducted. Singh *et al.* (1973) conducted experimental studies of the effective thermal conductivity of liquid saturated sintered fiber metal wicks, and a new correlation for predicting the effective thermal conductivity was proposed. Koh and Fortini (1973) performed experimental studies for prediction of thermal conductivity and electrical resistivity of porous materials including 304L stainless steel powders and OFHC sintered spherical powders. The results showed that the thermal conductivity and electrical resistivity could be related to the solid material properties and porosity of the porous matrix, regardless of the matrix structure. Hadley (1986) presented both experimental measurements and a theoretical model for the thermal conductivity of a consolidated mixture of a two-metal powder. The predictions showed good agreement with published two-phase data from a wide variety of sources. Shonnard and Whitaker (1989) conducted an experimental study to determine the effective thermal conductivity for a point-contact porous medium, and the results verified the functional dependence of (k_s/k_f) predicted by Batchelor and O'Brien. Besides, the experimental data and the theory of Batchelor and O'Brien were in good agreement with the experimental results of Swift. Prasad *et al.* (1989) conducted an experimental study to evaluate a correlation for stagnant thermal conductivity of liquid-saturated porous beds of spheres. The results showed that a mixing rule based on the volume fraction could not be used to predict stagnant thermal conductivity unless the thermal conductivity ratio was almost unity.

Differing with the above literature, Renken and Aboye (1993) analyzed film conductivity condensation within inclined thin porous-layer coated surfaces. The dependence of the average heat transfer coefficient on the surface subcooling, the gravity field and the thin porous-layer coating characteristics were documented.

Based on the above research, the temperature and concentration boundary conditions on the surfaces are almost always designated as respective constants. However, for some situations, such as the enhancement of a heat surface wetted with liquid, and evaporation of sweat on skin, etc, the temperature and concentration boundary conditions induced by evaporation of liquid on the heat surface can no longer be regarded as constants in advance, and mutual conjugation often results. The heat transfer mechanism of the above situations becomes complicated and is hard to investigate.

The purpose of this paper is to numerically investigate double diffusive natural convection phenomena of an enclosure filled with a porous medium. The channeling effect, constant porosity and Darcy-Brinkman-Forchheimer model of the porous medium are taken into consideration. To reduce the temperature on the heat wall, the heat wall is wetted with a thin water film. Due to the occurrence of latent and sensible heat transfer on the left wall, the boundary conditions of temperature and concentration of the heat wall are no longer designated as the known values in advance, and the above boundary conditions are then conjugated. The SIMPLEC numerical method is adopted to solve the governing equations and iterative computing processes are indispensable in obtaining temperatures, concentrations and velocities on the heat surface and in the enclosure. The results indicate that the effect of the evaporation on the reduction of temperature of the heat wall is remarkable and the latent heat transfer plays an important role in the heat transfer mechanism under high Darcy number situations. The relationship of averaged Nusselt number with Darcy-Rayleigh numbers is almost linear in logarithmic scale for high Darcy-Rayleigh numbers and the averaged Nusselt number

is approximately 2.5 for low Darcy-Rayleigh numbers.

II. PHYSICAL MODEL

A physical model of a two-dimensional rectengular enclosure filled with a porous medium is shown in Fig. 1. The width and length of the enclosure are labeled H and L, respectively. The gravity is downward and two horizontal walls of the enclosure are adiabatic. The left wall is subject to a uniform heat flux q_w and the relatively low temperature, concentration, and relative humidity conditions of the right wall are designated as T_R, C_R and ϕ_R, respectively, and are constant. In order to enhance the heat transfer rate of the left wall, the left wall surface is wetted with a water film. The thickness of the a water film is assumed to be extremely thin and stationary such that water does not penetrate into the region of the porous medium. The water film is evaporated by the heat flux imposed on the left wall and the condition of relative humidity of the left wall surface is saturated. Consequently, the sensible and latent heat transfers of natural convection occur in the enclosure simultaneously, and the temperature, $T_L(y)$ and concentration, $C_L(y)$ on the left wall are no longer regarded as constant in advance and conjugate mutually. The working fluid in the enclosure becomes an air-moist fluid.

To facilitate the analysis, the following assumptions are made .

(i) The porous medium is made of non-deformable pure copper spherical beads (k_s=386 $Wm^{-1}{}^{\circ}C^{-1}$) which are not chemically reactive with the fluid.

(ii) The flow in the enclosure is laminar, steady and two-dimensional. Corresponding to the thermal and concentration boundary conditions selected, condensation phenomenon does not occur in the enclosure.

(iii) The effects of Soret and Dufour induced by mass transfer are neglected, and Boussinesq approximation is held.

(iv) Except for the left wall region, the properties of the porous medium are constant and based on the temperature of the right wall. The properties on the left wall are based on the temperature of the left wall under a saturated condition (Kato and Mihara, 1977).

(v) The form of the effective thermal conductivity k_{eff} defined in Eq. (1) has been proposed in (Shonnand and Whitaker, 1989). The calculations of the air-moist fluid properties are shown in the the Appendix (Kato and Mihara, 1977). The porosity ε is constant and the permeability K and inertia factor F (Uafai, 1984) are defined in Eqs. (2) and (3), respectively.

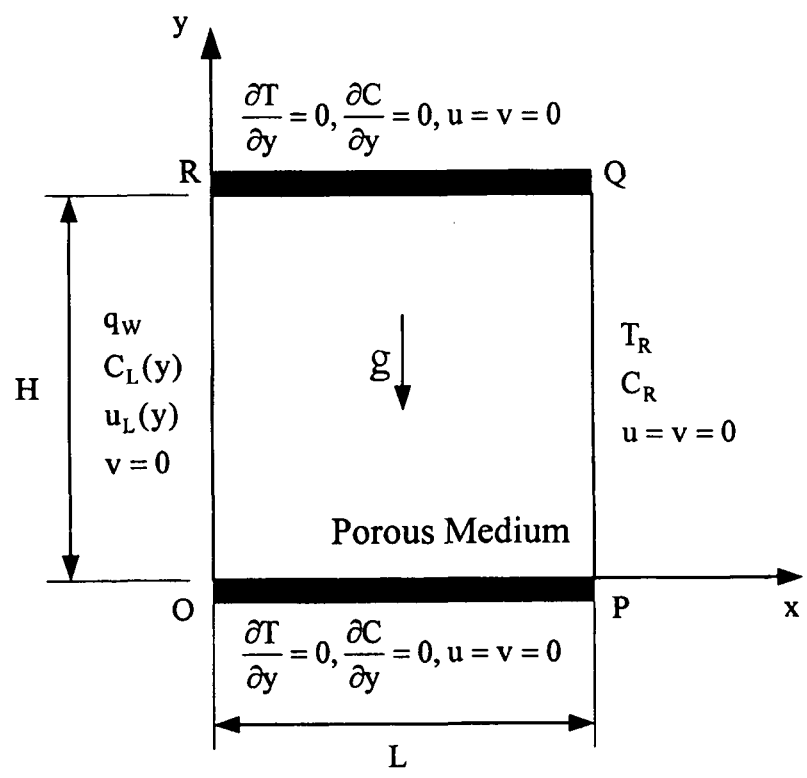

Fig. 1. Physical model.

$$k_{eff}=k_f[4\ln(\frac{k_s}{k_f})-11] \tag{1}$$

$$K=\frac{\varepsilon^3 d_p^2}{150(1-\varepsilon)^2} \tag{2}$$

$$F=\frac{1.75}{\sqrt{150}\varepsilon^{1.5}} \tag{3}$$

Based on the above assumptions and with the following characteristic scales of H, T_R, q_w, v_R, and k_{eff}, the governing equations adopted in (Hsiao *et al.*, 1992), geometry dimensions and boundary conditions are normalized as follows. The Darcy-Brinkman-Forchheimer model is used in the momentum equations.

Continuity equation

$$\frac{\partial U}{\partial X}+\frac{\partial V}{\partial Y}=0 \tag{4}$$

X-momentum equation

$$U\frac{\partial}{\partial X}(\frac{U}{\varepsilon})+V\frac{\partial}{\partial Y}(\frac{U}{\varepsilon})$$

$$=-\frac{\partial P}{\partial X}+(\frac{\partial^2 U}{\partial X^2}+\frac{\partial^2 U}{\partial Y^2})-\frac{1}{Da}\varepsilon U-\frac{F|\overrightarrow{U}|}{\sqrt{Da}}\varepsilon U \tag{5}$$

Y-momentum equation

$$U\frac{\partial}{\partial X}(\frac{V}{\varepsilon})+V\frac{\partial}{\partial Y}(\frac{V}{\varepsilon})=-\frac{\partial P}{\partial Y}+(\frac{\partial^2 V}{\partial X^2}+\frac{\partial^2 V}{\partial Y^2})-\frac{1}{Da}\varepsilon V$$

$$-\frac{F|\overrightarrow{U}|}{\sqrt{Da}}\varepsilon V+Gr_t\theta\varepsilon+Gr_c W\varepsilon \tag{6}$$

Energy equation

$$U\frac{\partial\theta}{\partial X}+V\frac{\partial\theta}{\partial Y}=\frac{1}{\mathrm{Pr}}\left(\frac{\partial^2\theta}{\partial X^2}+\frac{\partial^2\theta}{\partial Y^2}\right) \tag{7}$$

Concentration equation

$$U\frac{\partial W}{\partial X}+V\frac{\partial W}{\partial Y}=\frac{1}{Sc}\left(\frac{\partial^2 W}{\partial X^2}+\frac{\partial^2 W}{\partial Y^2}\right) \tag{8}$$

where

$$X=\frac{x}{H},\quad Y=\frac{y}{H},\quad U=\frac{uH}{\nu_R},\quad V=\frac{vH}{\nu_R},\quad P=\frac{pH^2}{\rho\nu_R^2}$$

$$\theta=\frac{k_{eff}(T-T_R)}{q_w H},\quad W=\frac{(C-C_R)}{(C_L(y)-C_R)}$$

$$Gr_t=\frac{g\beta_t q_w H^4}{k_{eff}\nu_R^2},\quad Gr_c=\frac{g\beta_c(C-C_R)H^3}{\nu_R^2} \tag{9}$$

$$\mathrm{Pr}=\frac{\nu_R}{\alpha_R},\quad Sc=\frac{\nu_R}{D_R},\quad \alpha=\frac{k_{eff}}{\rho Cp},\quad Da=\frac{K}{H^2}$$

$$\left|\overline{U}\right|=\sqrt{U^2+V^2}$$

Boundary conditions

On OP (top wall)

$$U=0,\ V=0,\ \frac{\partial\theta}{\partial Y}=0,\ \ \frac{\partial W}{\partial Y}=0 \tag{10}$$

On PQ (right wall)

$$U_R=0,\ V_R=0,\ \theta_R=0,\ W_R=0 \tag{11}$$

On QR (bottom wall)

$$U=0,\ V=0,\ \frac{\partial\theta}{\partial Y}=0,\ \ \frac{\partial W}{\partial Y}=0 \tag{12}$$

On RO (left wall)

$$U_L=\frac{u_L(y)H}{\nu_R}\quad V_L=0,\ \theta_L=\theta_L(Y),\ W_L=W_L(Y) \tag{13}$$

The other important values of evaporation mass flow rate $\dot{m}_L(y)$, evaporation velocity $u_L(y)$, sensible heat flux $q_s(y)$ and latent heat flux $q_\ell(y)$are calculated by the following equations, respectively

$$\dot{m}_L(y)=-\frac{\rho_L D_L}{(1-C_L(y))}\frac{\partial C}{\partial x}\bigg|_{x=0}$$

$$=-\frac{\rho_L D_L}{(1-C_L(y))}\frac{(C_E(x_1,y)-C_E(y))}{\frac{1}{2}\Delta x_1} \tag{14}$$

$$u_L(y)=\frac{\dot{m}_L(y)}{\rho_L}=\frac{-D_L}{(1-C_L(y))}\frac{\partial C}{\partial x}\bigg|_{x=0}$$

$$=-\frac{D_L}{(1-C_L(y))}\frac{(C_E(x_1,y)-C_L(y))}{\frac{1}{2}\Delta x_1} \tag{15}$$

$$q_w=q_s(y)+q_\ell(y) \tag{16}$$

$$q_s(y)=-k_{eff}\frac{\partial T}{\partial x}\bigg|_{x=0}=-k_{eff}\frac{(T_E(x_1,y)-T_L(y))}{\frac{1}{2}\Delta x_1} \tag{17}$$

$$q_\ell(y)=\dot{m}_L(y)h_{fg}=-\frac{\rho_L D_L h_{fg}}{(1-C_L(y))}\frac{\partial C}{\partial x}\bigg|_{x=0}$$

$$=-\frac{\rho_L D_L h_{fg}}{(1-C_L(y))}\frac{(C_E(x_1,y)-C_L(y))}{\frac{1}{2}\Delta x_1} \tag{18}$$

III. NUMERICAL METHOD

The SIMPLEC algorithm (Van Doormaal and Raithby, 1984) with TDMA solver (Patankas, 1980) is used to solve the governing Eqs. (3)-(8) of the flow, temperature and concentration fields. Eqs. (3)-(8) are first discretized into algebraic equations by using the control volume method (Patankar, 1980) with the power-law scheme. The under-relaxation factors for the velocity, temperature, and concentration fields range from 0.1~0.5 for all the fields. The conservation residues (Van Doormaal and Raithby, 1984) of the equations of momentum, energy, concentration and continuity and the relative errors of all variables are used to examine the convergence criteria which are defined as follows:

$$\left(\Sigma\left|\text{Re sidue of }\Phi\text{ equation}\right|_{\text{C.V.}}^2\right)^{1/2}\le 10^{-4},\ \Phi=U,\ V,\ \theta,\ W \tag{19}$$

$$\frac{\max\left|\Phi^{n+1}-\Phi^n\right|}{\max\left|\Phi^{n+1}\right|}\le 10^{-5},\ \Phi=U,\ V,\ P,\ \theta,\ W \tag{20}$$

To reduce computation time, staggered mesh is used, and the finer meshes are set near the solid wall regions. The meshes are then expanded outward from the boundary wall with a scale of 1.03. The accuracy of a similar numerical method is validated in Fu *et al.* (1996, 1997). A comparison of the results, which indicate double diffusive natural convection in a porous cavity with aspect ratio A=1 and Darcy number $Da=10^{-7}$ using the Darcy-Brinkman formulation of Goyeau *et al.* (1996), with the present method in shown in Table 1. The deviations between these two

Table 1. A comparison of the results of Goyeau *et al.* [21] with the present study.

Ra^*	Le	Nu (Goyeau *et al.*)	Nu (present study)	Error (%)	Sh (Goyeau *et al.*)	Sh (present study)	Error (%)
50	1	1.98	1.9984	0.92	1.98	1.9984	0.92
	10	1.98	1.9984	0.92	8.79	8.9514	1.8
	100	1.98	1.9984	0.92	27.97	28.754	2.73
100	1	3.11	3.1558	1.45	3.11	3.1558	1.45
	10	3.11	3.1558	1.45	13.25	13.660	3.00
	20	3.11	3.1558	1.45	18.89	19.558	3.42
	50	3.11	3.1558	1.45	29.72	30.619	2.94
	100	3.11	3.1558	1.45	41.53	42.358	1.95
200	1	4.96	5.0911	2.58	4.96	5.0911	2.58
	10	4.96	5.0911	2.58	19.86	20.615	3.66
	20	4.96	5.0911	2.58	28.17	29.083	3.12
	50	4.96	5.0911	2.58	44.00	44.658	1.47
	100	4.96	5.0911	2.58	61.09	60.327	1.26

methods are less than 4%.

The following steps provide a brief outline of the computing processes and numerical results based on the given data of T_R=293K, P_R=1.013 bar and ϕ_R=30%.

(i) Under given heat flux q_W and boundary conditions on the right wall, the pseudo values of T^n, C^n, u^n and v^n in the enclosure, including the left wall, are initially selected (n=0). Subsequently, calculate the corresponding properties of the air-moist fluid on the left wall including v_L^n, ρ_L^n, Cp_L^n, D_L^n and h_{fg}^n.

(ii) Based on the above conditions, utilize the SIMPLEC method to solve Eqs. (5) and (6) and obtain the values of $u_E^{n+1}(x,y)$ and $v_E^{n+1}(x,y)$ in the enclosure, without including the values on the left wall.

(iii) Based on the values of $u_E^{n+1}(x,y)$ and $v_E^{n+1}(x,y)$, the SIMPLEC method is successively utilized to solve Eqs. (7) and (8) to gain the new values of $T_E^{n+1}(x_1,y)$ and $C_E^{n+1}(x_1,y)$ in the enclosure except the values on the left wall.

(iv) Substitute $C_L^n(y)$ and $C_E^{n+1}(x_1,y)$ into Eq. (14) to calculate the evaporation mass flow rate $\dot{m}_L^n(y)$ on the left wall, and use Eq. (18) to obtain q_ℓ^n sequentially. If q_ℓ^n is smaller than q_W, continue the computing procedures, otherwise try a new value of $T_L(y)$and return to Step (ii).

(v) Subtract q_ℓ^n from q_W in Eq.(16) to obtain q_s^n. Use q_s^n in Eq. (17) to calculate $T_L^{n+1}(y)$ on the left wall.

(vi) Using the saturated condition on the left wall and the calculated value of $T_L^{n+1}(y)$, the new values of $C_L^{n+1}(y)$, $v_L^{n+1}(y)$, $\rho_L^{n+1}(y)$, $C_{\rho_L}^{n+1}(y)$, $D_L^{n+1}(y)$ and $h_{fg}^{n+1}(y)$ are calculated. Then $\dot{m}_L^{n+1}(y)$ can be calculated by the utilization of $C_L^{n+1}(y)$ and $C_E^{n+1}(x_1,y)$ in Eq. (14), and the evaporation velocity $u_L^{n+1}(y)$, induced by the evaporation mass flow rate $\dot{m}_L^{n+1}(y)$, is calculated from Eq. (15).

(vii) Calculate the values of $q_\ell^{n+1}(y)$ from Eq. (18), then subtract $q_\ell^{n+1}(y)$ from q_W in Eq. (16) and obtain $q_s^{n+1}(y)$.

(viii) Compare the values of $q_s^{n+1}(y)$ and $q_s^n(y)$ obtained from Steps (7) and (5), respectively. If the difference between $q_s^{n+1}(y)$ and $q_s^n(y)$ and the convergence criteria of $T_E(x,y)$, $C_E(x,y)$, $u_E(x,y)$ and $v_E(x,y)$ do not satisfy the criteria of Eqs. (21) and (19)~(20), respectively, then use the corrected values of $T_L^{n+1}(y)$, $C_L^{n+1}(y)$, $u_L^{n+1}(y)$ and the corresponding properties T_E^{n+1}, C_E^{n+1}, u_E^{n+1}, v_E^{n+1} of air-moist fluid to iterate the computing procedure from Step (2), until the above conditions are satisfied.

$$\frac{\left|q_s^{n+1}-q_s^n\right|}{q_s^{n+1}} \le 10^{-3} \tag{21}$$

IV. RESULTS AND DISCUSSIONS

The dimensionless parameters of four Rayleigh numbers, three porosities and three diameters of spherical beads tabulated in Table 2 are adopted in this paper. H, L, T_R=293K, ϕ_R=30%, Pr=0.02583 and Sc=0.5425 are fixed in the following situations. The ranges of Ra^* and Da are from 0.02725 to 4469.041 and from 2.963×10^{-8} to 1.215×10^{-3}, respectively.

The grid test for computation is based on the situation of Ra=9.197×10^5, Dp=5×10^{-3} and ε=0.4. The results of the test are listed in Table 3, and

Table 2. Values of *Ra*, ε and *Dp* adopted in the study.

Ra	ε	*Dp*
9.197×10^5	0.4	0.005
1.839×10^6	0.7	0.025
2.758×10^6	0.9	0.05
3.678×10^6		

Table 3. Grid tests for $Ra=9.197\times10^5$, $\varepsilon=0.4$, and $Dp=0.005$

Δ_{x1},Δ_{y1}	Ratio $(\frac{\Delta x_{i+1}}{x_i})$	Grids ($Nx\times Nv$)	$\overline{Nu}$
0.025	1.03	32×32	0.99562
0.025	1.01	36×36	0.99578
0.015	1.005	38×38	0.99570
0.015	1.03	46×46	0.99650
0.015	1.01	58×58	0.9951
0.01	1.03	62×62	0.9959
0.01	1.001	98×98	0.9955
0.0075	1.05	60×60	0.9956
0.0075	1.03	74×74	0.9967
0.0075	1.01	102×102	0.9955
0.0075	1.005	116×116	0.9955
0.005	1.03	94×94	0.9961
0.0025	1.05	98×98	0.9961
0.0025	1.03	132×132	0.9969

the grids of 74×74 are selected for the following calculation processes with $\Delta x_1=\Delta y_1=0.0075$ and the ratio of $\Delta x_{i+1}/\Delta x_i=1.03$, which are symmetric to central lines of the computing domain.

The distributions of streamlines, isothermal lines and constant concentration lines are illustrated in Fig. 2. In Figs. 2(a) and (b), as *Ra* becomes larger, the convection is more dominant, the isothermal lines become more skewed and the distributions of concentration lines are dense near the two vertical walls of Fig. 2(b).

In Figs. 2(c) and (d), the larger the porosity is, the stronger the convection becomes, therefore, the isothermal and concentration lines of Fig. 2(d) are more curved than these shown in Fig. 2(c). For the same reason, the larger the diameter of the spherical bead, the more dominant the convection, and the distributions of the isothermal and concentration lines of Fig. 2(f) are more skewed than these of Fig. 2(e).

The distributions of modified dimension temperature θ^* on the left wall under different physical situations are illustrated in Fig. 3. The situations shown in Figs. 3(a) and 3(b) are the two limiting cases

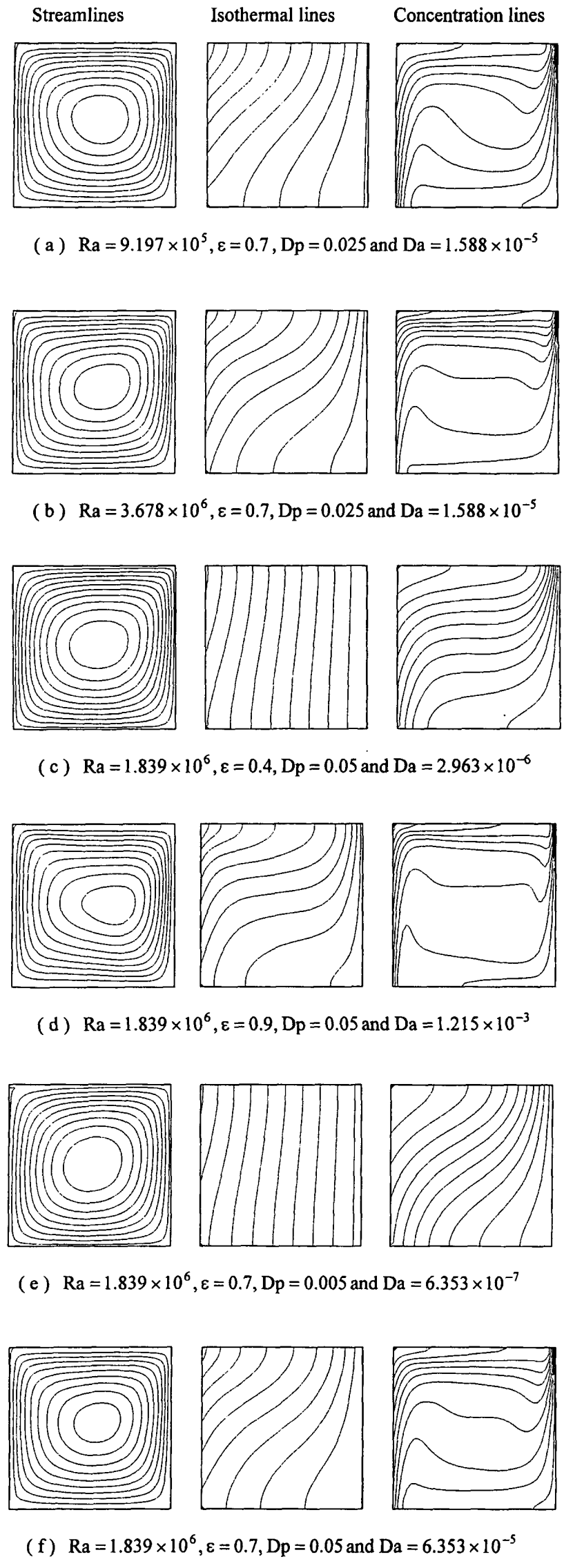

Fig. 2. The distributions of streamlines, isothermal lines and constant concentration lines under different Rayleigh numbers *Ra*, porosities ε and diameters of beads *Dp*.

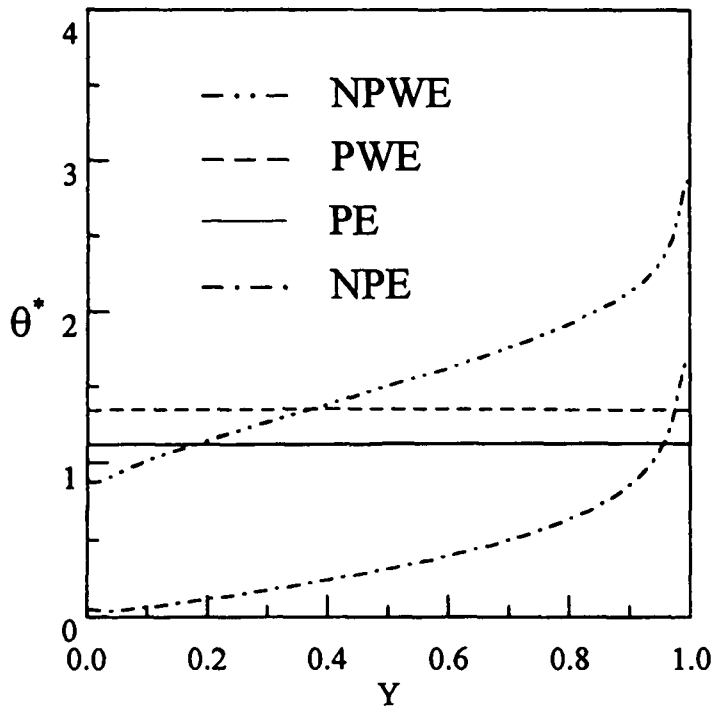

(a) Ra=9.197×10^5, ε=0.4, Dp=0.005 and Da=2.963×10^{-8}

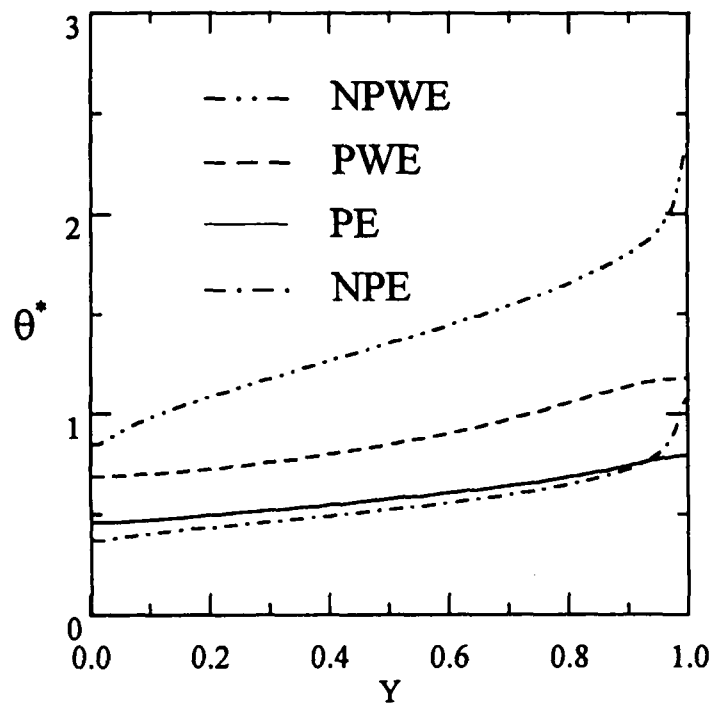

(b) Ra=3.678×10^6, ε=0.9, Dp=0.05 and Da=1.215×10^{-3}

Fig. 3. The distributions of modified dimensional temperature θ^* on the left wall under four different physical situations.

of convection capability under the lowest and highest Ra^*, respectively. Generally, the effect of the evaporation on heat transfer is remarkable, and then the temperatures distributed on the left wall descend efficiently. The flow resistance in the porous medium situation (PE) is greater than that in the non-porous medium situation (NPE), therefore convection in the NPE situation is more active than that in the PE situation. As a result, for most regions of the left wall, the temperatures of the NPE situation are lower than those of the PE situation. However, the convection effect is weak in the upper region of the left wall (the upper left corner). The occurrence of conduction in the PE situation, with a larger thermal conductivity ratio $(\frac{k_s}{k_f})$ in upper region of the left wall, is more remarkable than that of the NPE situation. The highest temperature of the PE situation in upper region of the left wall is lower than that of the NPE case, and the distribution of temperature is more even than that of the NPE case.

The effects of Rayleigh number Ra, porosity ε and diameter of bead Dp on the local Nusselt $Nu(Y)$ and Sherwood numbers $Sh(Y)$ on the left wall are illustrated in Figs. 4(a), 4(b) and 4(c), respectively. The definitions of $Nu(Y)$ and $Sh(Y)$ are expressed in the following equations.

$$Nu(Y)=\frac{h_t(y)H}{k_{eff}}=Nu_s(Y)+Nu_\ell(Y)$$

$$=\frac{q_s}{q_w}\frac{1}{\theta_L(Y)}+\frac{q_\ell}{q_w}\frac{1}{\theta_L(Y)} \qquad (22)$$

where $h_t(y)=\dfrac{q_w}{(T_L(y)-T_R)}$

$$Sh(Y)=\frac{h_c(y)H}{D_L}=-\left.\frac{\partial W}{\partial X}\right|_{X=0} \qquad (23)$$

where $h_c(y)=\dfrac{\dot{m}_L(1-C_L(y))}{\rho_L(C_L(y)-C_R)}$

In general, as Ra, ε and Dp become larger, evaporation, mainly induced by convection, becomes more dominant. Therefore, the local Nusselt and Sherwood numbers on the left wall are larger under the larger Ra, ε and Dp situations.

In Fig. 5, the values of R_ℓ and q_s indicate the ratios of latent heat flux q_ℓ and sensible heat flux q_s to the total heat flux q_w, respectively, and these values are defined in the following equations.

$$R_\ell=\frac{q_\ell}{q_w} \text{ and } R_s=\frac{q_s}{q_w} \qquad (24)$$

The value of the ratio R means the contribution of above individual heat flux to the total heat flux. As the values of Ra, ε and Dp become smaller, the resistance to fluid flow becomes serious, which simultaneously results in weak convection and little evaporation. The value of R_ℓ is thus smaller under the smaller Ra, ε and Dp cases as shown in Figs. 5 (a1), 5(a2) and 5(a3). Oppositely, as the values of Ra, ε and Dp become larger, based on the reason mentioned above, evaporation becomes dominant and the values of R_ℓ are larger as shown in Figs. 5(b2), 5(c2) and 5(c3). In Fig. 5(c2), the value of R_ℓ is even larger than 1 at $Y\approx0.03$ which means the evaporation of film absorbs heat not only from the total heat flux q_w on the left wall but also from the

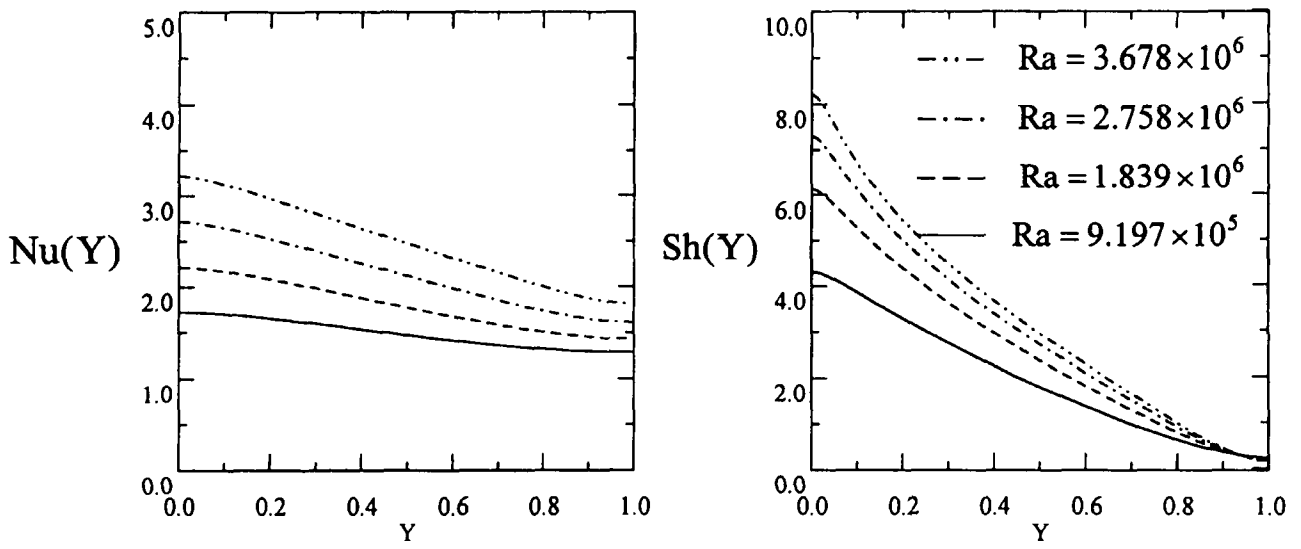

(a) $\varepsilon = 0.4$, $Dp = 0.05$ and $Da = 2.963 \times 10^{-6}$

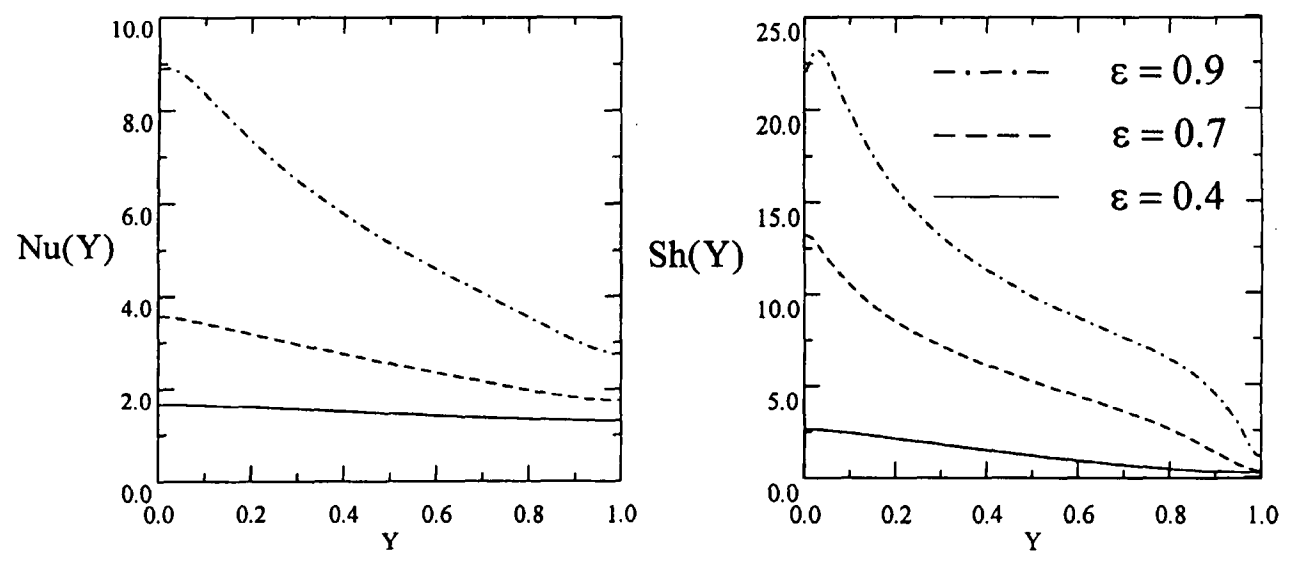

(b) $Ra = 1.839 \times 10^6$ and $Dp = 0.025$

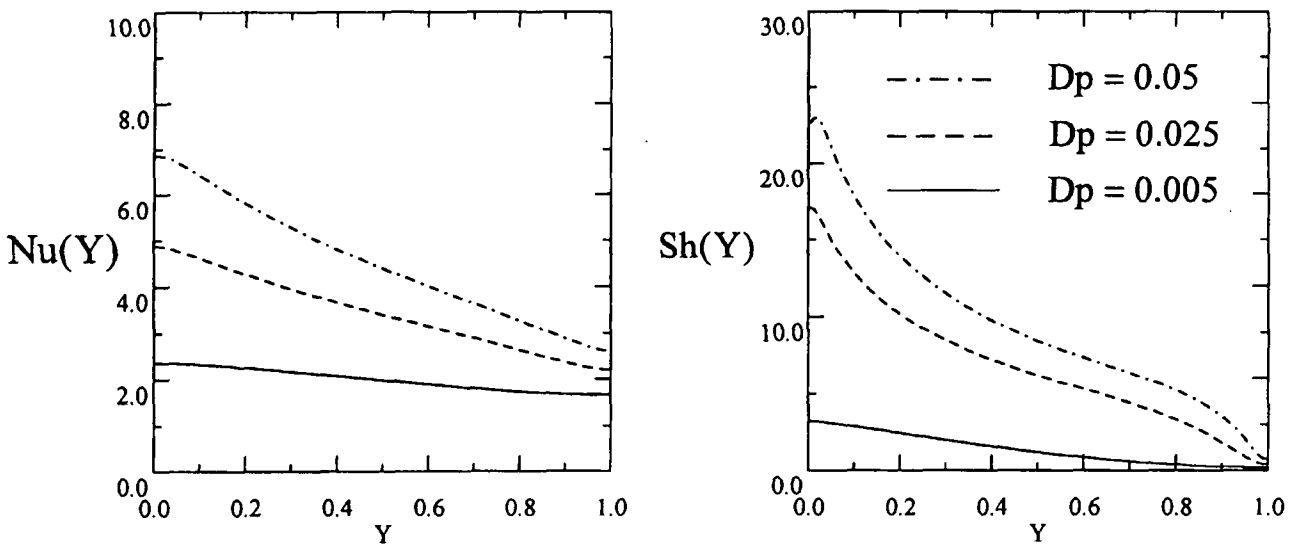

(c) $Ra = 3.678 \times 10^6$ and $\varepsilon = 0.7$

Fig. 4. The distributions of local Nusselt and Sherwood numbers on the left wall.

fluid in the enclosure. As *Dp* or ε increases, *Da* also increases, which leads to greater permeability of the porous medium and an increase in latent heat transfer. Based on the above results, the latent heat flux plays an important role in the heat transfer mechanism under a high Darcy number. Besides, the distribution of the ratio R_ρ in the low Rayleigh number region is larger than that in the high Rayleigh number region under $Da > 10^{-5}$.

The distributions of velocity *U* along the *Y*-axis at *X*=0.0075 are very close to the left wall are shown in Fig. 6. The evaporation of the water film on

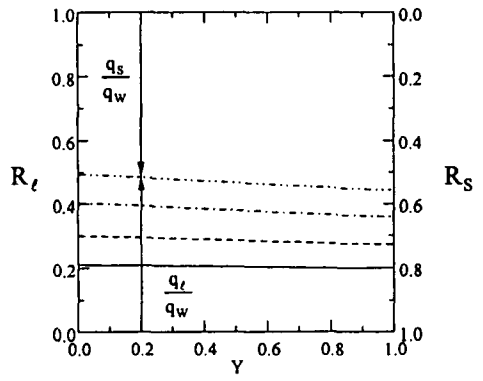

(a1) $\varepsilon = 0.4$, $Dp = 0.005$, $Da = 2.963 \times 10^{-8}$

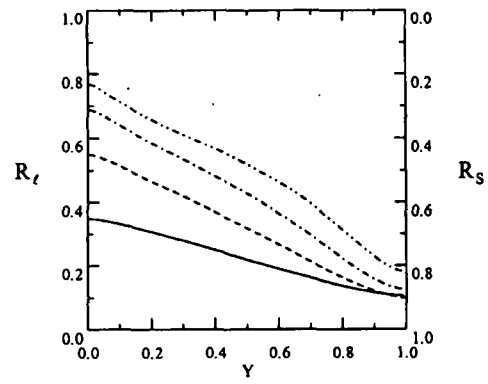

(a2) $\varepsilon = 0.4$, $Dp = 0.025$, $Da = 7.408 \times 10^{-7}$

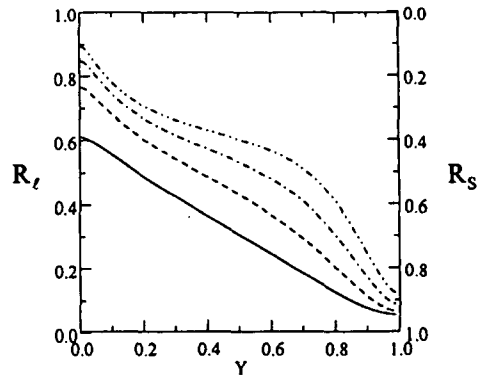

(a3) $\varepsilon = 0.4$, $Dp = 0.05$, $Da = 2.963 \times 10^{-6}$

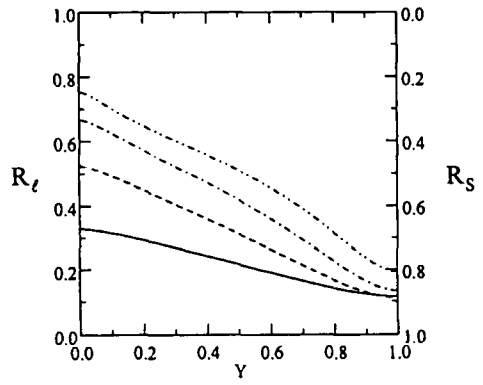

(b1) $\varepsilon = 0.7$, $Dp = 0.005$, $Da = 6.353 \times 10^{-7}$

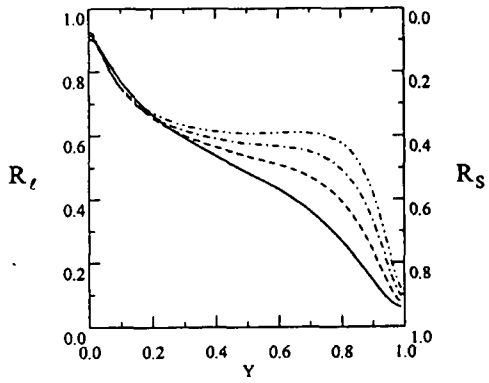

(b2) $\varepsilon = 0.7$, $Dp = 0.025$, $Da = 1.588 \times 10^{-5}$

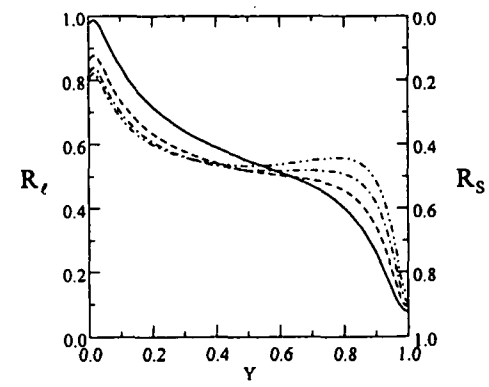

(b3) $\varepsilon = 0.7$, $Dp = 0.05$, $Da = 6.353 \times 10^{-5}$

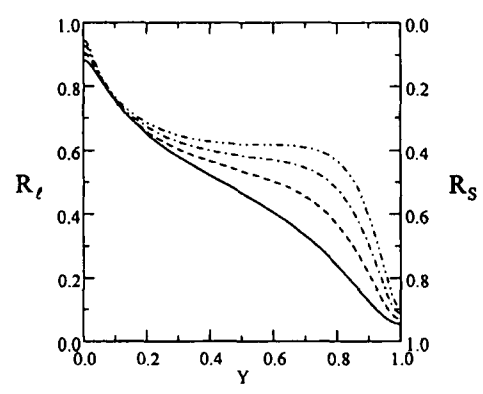

(c1) $\varepsilon = 0.9$, $Dp = 0.005$, $Da = 1.215 \times 10^{-5}$

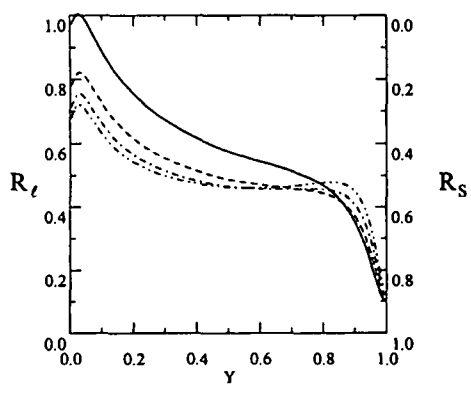

(c2) $\varepsilon = 0.9$, $Dp = 0.025$, $Da = 3.308 \times 10^{-4}$

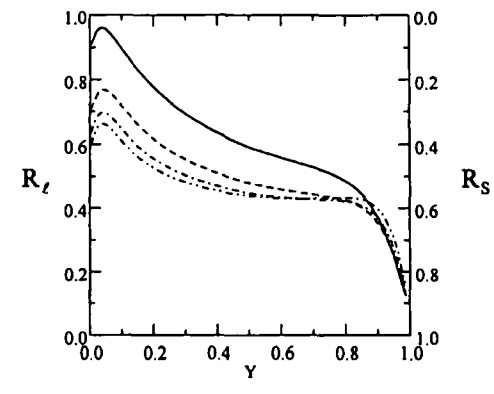

(c3) $\varepsilon = 0.9$, $Dp = 0.05$, $Da = 1.215 \times 10^{-3}$

Fig. 5. The distributions of R_ℓ and R_s on the left wall under different situations. (–··–Ra=3.678×10^6, –·–·Ra=2.758×10^6, – – –Ra=1.839×10^6, —Ra=9.197×10^5)

the left wall is taken into consideration, and the direction of the evaporation velocity $u_L(y)$ is to the right. Under the strong convection cases shown in Figs. 6(d), 6(e) and 6(f) mentioned earlier, the main velocity of the fluid flow in the enclosure is clockwise and overcomes the evaporation velocity, and the direction of the resultant velocity is to the left in the lower region of the Y axis. Oppositely, when ε=0.4 and Dp=5×10^{-3}, the convection effect is minute, and the evaporation velocity is relatively more remarkable than that of the fluid flow in the enclosure. Consequently, in this situation, the direction of the velocity U is to the right in the lower region of the Y-axis. In the upper region of the Y-axis, the direction of the main velocity of the fluid flow and the evaporation velocity are the same and to the right. Naturally, the direction of the velocity U is to the right in the upper region of the Y-axis, and the channeling effect is observed in some situations.

The distributions of velocity V along the X-axis at different positions at both vertical walls are illustrated in Fig. 7. The channeling effect is observed in some situations of Figs. 7(b), (d), (e) and (f) where the convection is strong. Due to the occurrence of evaporation on the left wall, the channeling effect on the right wall is more apparent than that on the left wall. For the same reason, as ε=0.4 and 0.7, and Dp=5×10^{-3}, the convection, and there is little evidence of the channeling effect on the both walls.

Figure 8 shows the relationship of Darcy-Rayleigh number Ra^* with the averaged Nusselt

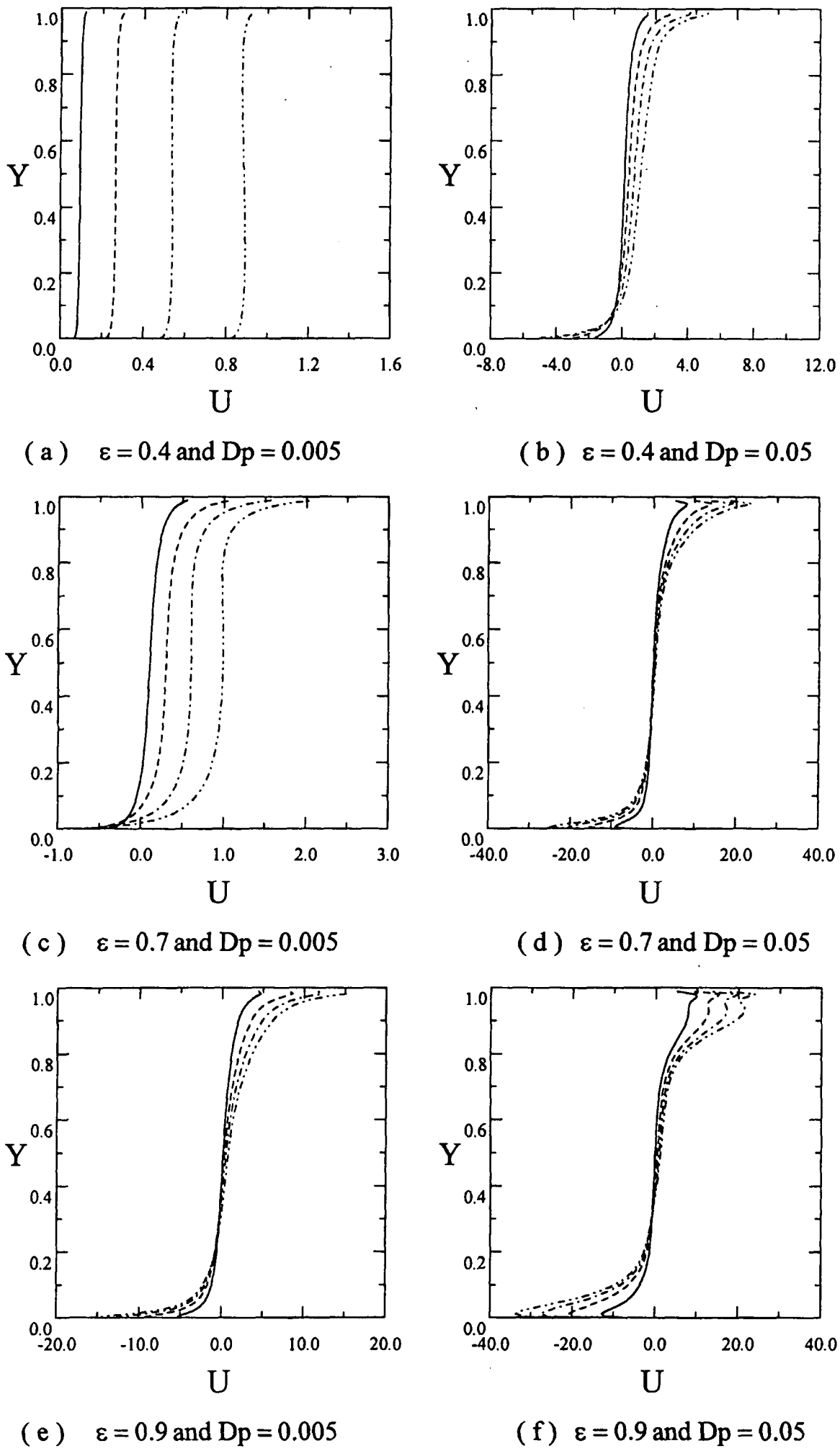

(a) $\varepsilon = 0.4$ and $Dp = 0.005$

(b) $\varepsilon = 0.4$ and $Dp = 0.05$

(c) $\varepsilon = 0.7$ and $Dp = 0.005$

(d) $\varepsilon = 0.7$ and $Dp = 0.05$

(e) $\varepsilon = 0.9$ and $Dp = 0.005$

(f) $\varepsilon = 0.9$ and $Dp = 0.05$

Fig. 6. The distributions of velocity U along the Y-axis at X=0.0075 under different situations. (–··–Ra=3.678×10^6, –·–·Ra=2.758×10^6, – – –Ra=1.839×10^6, —Ra=9.197×10^5)

number $\overline{Nu}$, which is defined in Eq. (25) and expressed in Eqs. (26) and (27). Under the smaller Ra^* regions, the averaged Nusselt number $\overline{Nu}$ is almost independent of the Darcy-Rayleigh number and its value is approximately 2.5. Beyond the above region, the relationship of $\overline{Nu}$ with Ra^* is almost linear based on the logarithmic coordinates. The equations of these two parts are shown in Eqs. (26)

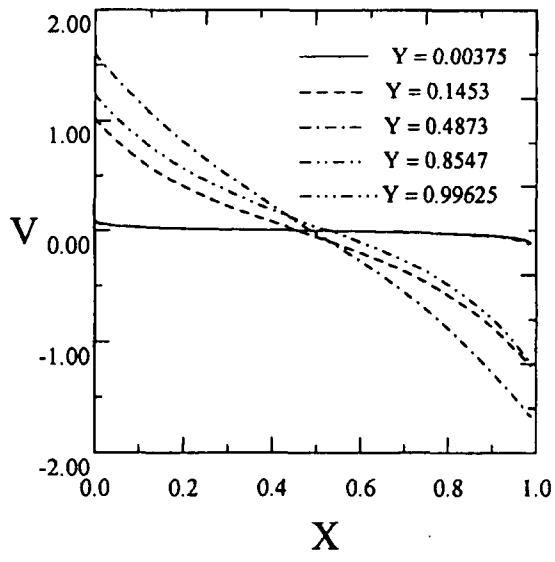

(a) ε = 0.4 and Dp = 0.005

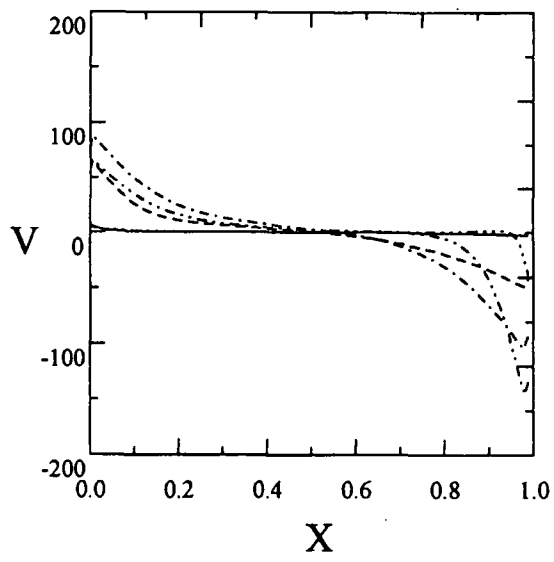

(b) ε = 0.4 and Dp = 0.05

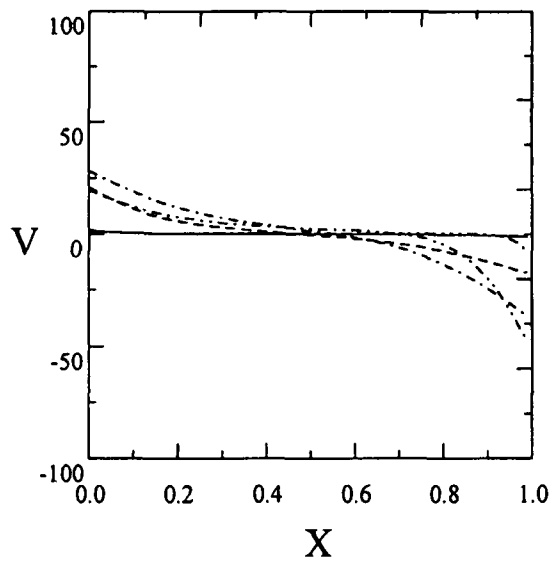

(c) ε = 0.7 and Dp = 0.005

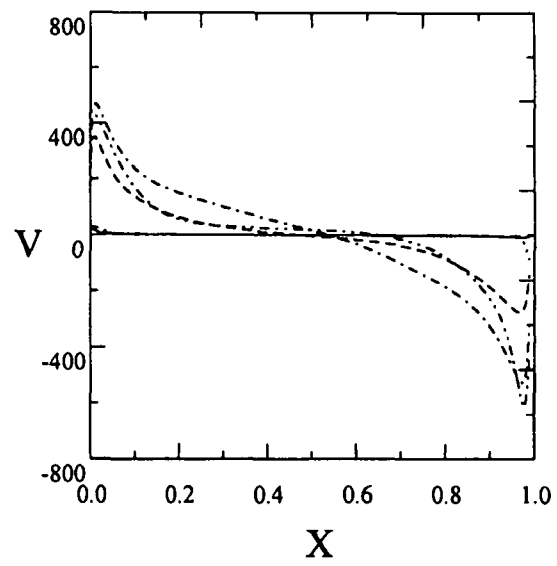

(d) ε = 0.7 and Dp = 0.05

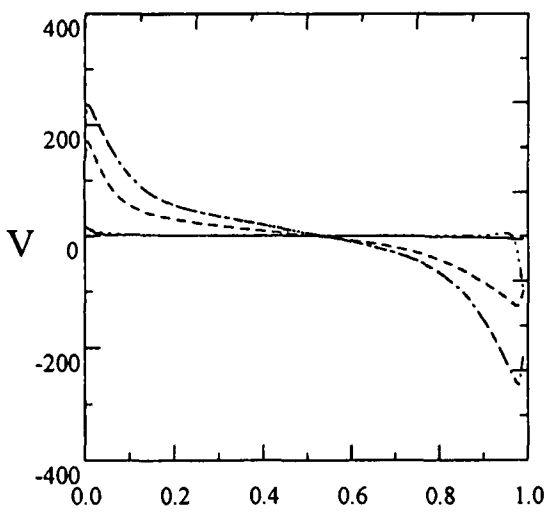

(e) ε = 0.9 and Dp = 0.005

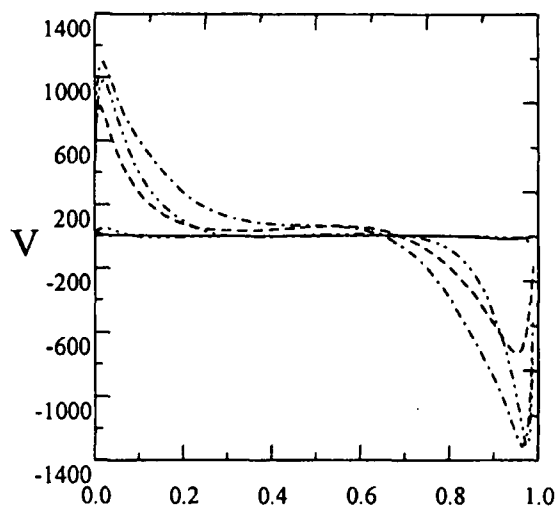

(f) ε = 0.9 and Dp = 0.05

Fig. 7. The distributions of velocity V along the X-axis at different heights of Y-axis under situation of Ra=3.678×10^6 situation.

and (27)

$$\overline{Nu} = \int_0^1 Nu(Y)dY \tag{25}$$

$$\overline{Nu} = 2.5 \pm 0.5 \text{ for } Ra^* \leq 4 \tag{26}$$

$$\overline{Nu} = 1.9463 Ra^{*0.202} \text{ for } 4 < Ra^* < 4469 \tag{27}$$

V. CONCLUSIONS

A double diffusive natural convection in an enclosure filled with a porous medium under an

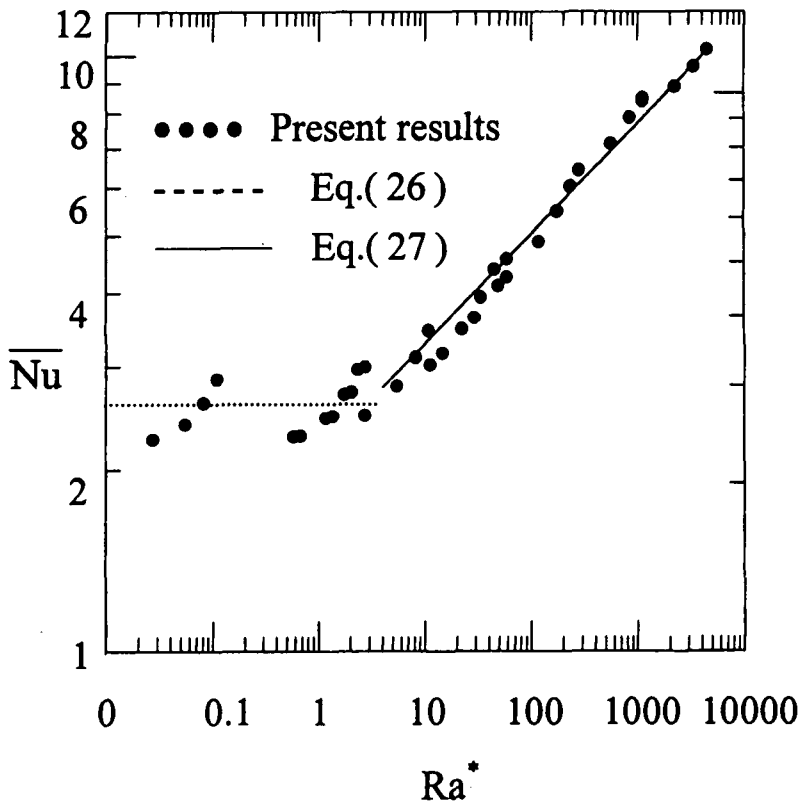

Fig. 8. The relationship of averaged Nusselt number $\overline{Nu}$ and Darcy-Rayleigh number Ra^*.

evaporation situation was investigated numerically. The effects of Rayleigh number Ra, porosity ε and diameter of beads Dp on heat transfer were examined with the D-B-F model. The results are summarized as follows:

(i) The effect of evaporation on the reduction of temperature of the heated wall is remarkable, especially in the upper corner.

(ii) The latent heat flux plays an important role in the heat transfer mechanism for high Darcy numbers. The distribution of the ratio R_ℓ in the lower Ra region is larger than that in the high Ra region as $Da>10^{-5}$.

(iii) The relationship of averaged Nusselt number $\overline{Nu}$ with Darcy-Rayleigh number Ra^* is almost linear in logarithmic scale when $4<Ra^*<4469$; and $\overline{Nu}$ is approximately 2.5 when $Ra^*<4$.

NOMENCLATURE

C	Mass or concentration fraction
Cp	Specific heat of fluid ($kJkg^{-1}\ °C^{-1}$)
dp	Porous bead diameter (m)
D	Binary diffusion coefficient (m^2s^{-1})
Da	Darcy number
Dp	Dimensionless porous bead diameter, (dp/H)
F	Inertial factor; Forchheimer factor
g	Gravitational acceleration (ms^{-2})
Gr_c	Grashof number for mass diffusion, $[g\beta_C(C-C_R)H^3)/\nu_R^2]$
Gr_t	Grashof number for thermal diffusion, $[(g\beta_t q_w H^4)/(k_{eff}\nu_R^2)]$
h_c	Mass transfer coefficient along vertical wall
h_{fg}	Vaporization enthalpy (Jkg^{-1})
h_t	Thermal heat transfer coefficient along vertical wall ($Wm^{-2}\ °C^{-1}$)
H	Dimensional width of porous enclosure (m)
k_{eff}	Effective thermal conductivity of porous medium ($Wm^{-1}\ °C^{-1}$)
k_f	Thermal conductivity of fluid ($Wm^{-1}\ °C^{-1}$)
k_s	Thermal conductivity of solid phase in porous medium ($Wm^{-1}\ °C^{-1}$)
K	Permeability (m^2)
L	Dimensional length of porous enclosure (m)
$\dot{m}$	Evaporation mass flow rate ($Kgm^{-2}s^{-1}$)
Nu	Local Nusselt number along vertical wall
$\overline{Nu}$	Mean Nusselt number
p	Dimensional pressure (Nm^{-2})
P	Dimensionless pressure
Pr	Prandtl number
q_W	Heat flux (Wm^{-2})
Ra	Rayleigh number, $[Gr_t\ Pr=(g\beta_t q_W H^4)/(k_{eff}\nu_R\alpha_R)]$
Ra^*	Darcy-Rayleigh number, $[RaDa=(g\beta_t q_W H^2 K)/(k_{eff}\nu_R\alpha_R)]$
R_ℓ	Ratio of latent heat flux in left wall to total heat flux in the left wall
R_s	Ratio of sensible heat flux in left wall to total heat flux in the left wall
Sc	Schmidt number, $(\frac{\nu}{D})$
Sh	Local Sherwood number along vertical wall
T	Temperature (°C)
u	Dimensional velocity in x direction (ms^{-1})
U	Dimensionless velocity in X direction
v	Dimensional velocity in y direction (ms^{-1})
V	Dimensionless velocity in Y direction
W	Dimensionless concentraction
x, y	Dimensional Cartesian coordinate (m)
X, Y	Dimensionless Cartesian coordinate, $(=x/H, =y/H)$
PE	Porous medium with evaporation situation in enclosure
PWE	Porous medium without evaporation situation in enclosure
NPE	Non-porous medium with evaporation situation in enclosure
$NPWE$	Non-porous medium without evaporation situation in enclosure

Greek symbols

α	Thermal diffusivity (m^2s^{-1})
β_t	Coefficient of volumetric expansion with temperature ($°C^{-1}$)
β_c	Coefficient of volumetric expansion with mass fraction

ε	Porosity (m^3m^{-3})
μ	Viscosity ($kgm^{-1}s^{-1}$)
ν	Kinematic viscosity (m^2s^{-1})
θ	Dimensionless temperature
θ^*	Modified dimension temperature (θ/k_{eff}) ($W^{-1}m$ °C)
ρ	Fluid density (kgm^{-3})
ϕ	Relative humidity
Φ	Computation variable
ψ	Dimensionless stream function

Superscripts

n	The nth iteration index
–	Mean value
$\rightarrow$	Velocity vector

Subscripts

C.V.	Control volume
eff	Effective value
E	Enclosure
f	Fluid phase
i	Index
ℓ	Latent heat
L	Left wall
p	Porous medium
R	Right wall
s	Solid phase
S	Sensible heat
W	Solid wall

OTHER

| |	Magnitude of velocity vector

ACKNOWLEDGMENT

The support of this work by the National Science Council, Taiwan, R.O.C. under contract NSC86-2212-E-009-042 is gratefully acknowledged. The authors also appreciate the instructive suggestions from Dr. Huang.

REFERENCES

1. Alavyoon, F., 1993, "On Natural Convection in Vertical Porous Enclosures Due to Prescribed Fluxes of Heat and Mass at the Vertical Boundaries," *International Journal of Heat and Mass Transfer*, Vol. 36, pp. 2479-2498.
2. Alavyoon, F., Masuda, Y. and Kimura, S., 1994, "On Natural Convection in Vertical Porous Enclosures Due to Opposing Fluxes of Heat and Mass Prescribed at the Vertical Walls," *International Journal of Heat and Mass Transfer*, Vol. 37, pp. 195-206.
3. Fu, W.S., Huang, H.C. and Liou, W.Y., 1996, "Thermal Enhancement in Laminar Channel Flow with a Porous Block," *International Journal of Heat and Mass Transfer*, Vol. 39, pp. 2165-2175.
4. Fu, W.S. and Huang, H.C., 1997, "Thermal Performances of Different Shapes of Porous Blocks under an Impinging Jet," *International Journal of Heat and Mass Transfer*, Vol. 40, pp. 2261-2272.
5. Fujii, T., Kato, Y. and Mihara, K, 1977, "Expression of Transport and Thermodynamic Properties of Air, Steam and Water," Sei San Ka Gaku Kenkyu Jo, Report no. 66, Kyu Shu Dai Gaku, Kyu Shu, Japan.
6. Goyeau, B., Songbe, J.P. and Gobin, D., 1996, "Numerical Study of Double-diffusive Natural Convection in a Porous Cavity Using the Darcy-Brinkman Formulation," *International Journal of Heat and Mass Transfer*, Vol. 39, pp. 1363-1378.
7. Hadley, G.R., 1986, "Thermal Conductivity of Packed Metal Powders," *International Journal of Heat and Mass Transfer*, Vol. 29, pp. 909-920.
8. Hsiao, S.W., Cheng, P. and Chen, C.K., 1992, "Non-uniform Porosity and Thermal Dispersion Effects on Natural Convection About a Heated Horizontal Cylinder in an Enclosed Porous Medium," *International Journal of Heat and Mass Transfer*, Vol. 35, pp. 3407-3418.
9. Kon, J.C.Y. and Fortini, A., 1973, "Prediction of Thermal Conductivity and Electrical Resistivity of Porous Metallic Materials," *International Journal of Heat and Mass Transfer*, Vol. 16, pp. 2013-2022.
10. Lai, F.C. and Kulacki, F.A., 1991, "Coupled Heat and Mass Transfer by Natural Convection from Vertical Surfaces in Porous Media," *International Journal of Heat and Mass Transfer*, Vol. 34, pp. 1189-1194.
11. Lauriat, G. and Prasad, V., 1989, "Non-Darcian Effects on Natural Convection in a Vertical Porous Enclosure," *International Journal of Heat and Mass Transfer*, Vol. 32, pp. 2135-2148.
12. Murray, B.T. and Chen, C.F., 1989, "Double-diffusive Convection in a Porous Medium," *Journal of Fluid Mechanics*, Vol. 201, pp. 147-166.
13. Nithiarasu, P., Seetharamu, K.N. and Sundararajan, T., 1997, "Natural Convective Heat Transfer in a Fluid Saturated Variable Porosity Medium," *International Journal of Heat and Mass Transfer*, Vol. 40, pp. 3955-3967.
14. Patankar, S.V., 1980, "Numerical Heat Transfer and Fluid Flows," Hemisphere, Washington

D.C.
15. Prasad, V., Kladias, N., Bandyopadhaya, A. and Tian, Q., 1989, "Evaluation of Correlations for Stagnant Thermal Conductivity of Liquid-saturated Porous Beds of Spheres," *International Journal of Heat and Mass Transfer*, Vol. 32, pp. 1793-1789.
16. Renken, K.J. and Aboye, M., 1993, "Analysis of Film Condensation Within Inclined Thin Porous-layer Coated Surfaces," *International Journal of Heat and Fluid Flow*, Vol. 14, pp. 48-53.
17. Shonnard, D.R. and Whitaker, S., 1989, "The Effective Thermal Conductivity for Point Contact Porous Medium: an Experimental Study," *International Journal of Heat and Mass Transfer*, Vol. 23, pp. 503-512.
18. Singh, B.S., Dybbs, A. and Lyman, F.A., 1973, "Experimental Study of the Effective Thermal Conductivity of Liquid Saturated Sintered Fiber Metal Wicks," *International Journal of Heat and Mass Transfer*, Vol. 16, pp. 145-155.
19. Trevisan, O.V. and Bejan, A., 1985, "Natural Convection with Combined Heat and Mass Transfer Buoyancy Effects in a Porous Medium," *International Journal of Heat and Mass Transfer*, Vol. 28, pp. 1597-1611.
20. Vafai, K., 1984, "Convection Flow and Heat Transfer in Variable Porosity Media," *Journal of Fluid Mechanics*, Vol. 147, pp. 233-259.
21. Van Doormaal, J.P. and Raithby, G.D., 1984, "Enhancements of the SIMPLE Method for Predicting Incompressible Fluid Flow," *Numerical Heat Transfer*, Vol. 7, pp. 147-163.

APPENDIX

Thermophysical properties of air, steam and air-moist mixture, in $T[K]$, $T[°C]$ and P[bar].

(i) Air

$$\rho_a=348.33\frac{P}{T} \quad (kgm^{-3})$$

$$\mu_a=1.488\times10^{-6}\frac{T^{1.5}}{118+T} \quad (kgm^{-1}s^{-1})$$

$$k_a=1.195\times10^{-3}\frac{T^{1.6}}{118+T} \quad (kgm^{-1}K^{-1})$$

$$CP_a=(1+2.5\times10^{-10}T^3)\times10^3 \quad (Jkg^{-1}K^{-1})$$

(ii) Steam

$$\rho_{stm}=2.167\times10^2[1+1.68(\frac{P}{T})^{0.8}](\frac{P}{T}) \quad (kgm^{-3})$$

$$\mu_{stm}=(8.02+0.04t)\times10^{-6} \quad (kgm^{-1}s^{-1})$$

$$k_{stm}=(1.87+1.65\times10^{-3}t^{9/7}+5.7\times10^{-13}t^{5.1})\times10^{-2} \quad (kgm^{-1}K^{-1})$$

$$CP_{stm}=1.863\times10^3+1.65\times10^{-3}t^{2.5}+1.2\times10^{-18}t^{8.5} \quad (Jkg^{-1}K^{-1})$$

(iii) Air-moist mixture

$$\rho_m=\frac{1+\omega}{[0.455(\omega+0.622)T]\times10^{-2}} \quad (kgm^{-3})$$

$$\mu_m=\frac{\mu_a}{1+0.352(1+0.8882\sqrt{\frac{\mu_a}{\mu_{stm}}})^2\frac{C}{1-C}}+\frac{\mu_{stm}}{1+0.1727(1+1.1259\sqrt{\frac{\mu_{stm}}{\mu_a}})^2\frac{1-C}{C}} \quad (kgm^{-1}s^{-1})$$

$$k_m=\frac{k_a}{1+0.4018\left\{1+0.837\left[\frac{\mu_a}{\mu_{stm}}\frac{(1+\frac{115.5}{T})}{(1+\frac{559.7}{T})}\right]^{\frac{1}{2}}\right\}^2\frac{(1+\frac{186.4}{T})}{(1+\frac{115.5}{T})}\frac{C}{1-C}}+\frac{k_{stm}}{1+0.15556\left\{1+1.195\left[\frac{\mu_{stm}}{\mu_a}\frac{(1+\frac{559.7}{T})}{(1+\frac{115.5}{T})}\right]^{\frac{1}{2}}\right\}^2\frac{(1+\frac{186.4}{T})}{(1+\frac{115.5}{T})}\frac{1-C}{C}} \quad (kgm^{-1}K^{-1})$$

$$Cp_m=(1-C)\cdot Cp_a+C\cdot Cp_{stm} \quad (\mathrm{Jkg^{-1}K^{-1}})$$

$$D_m=8.07\times10^{-6}T^{1.833} \quad (\mathrm{m^2s^{-1}})$$

(iv) Others

The evaporation latent heat from the liquid phase to vapor phase for water saturation

$$h_{fg}=4186.8\times(597.3-0.559t) \quad (\mathrm{Jkg^{-1}})$$

The saturation pressure of the vapor phase for water

$$Log_{10}(\frac{P_{sat}}{221.2})=-[3.1323+3.116\times10^{-6}\times(210-t)^{2.066}(\frac{647.3}{273.15+t}-1)]$$

Humidity ratio

$$\omega=\frac{0.622\phi P_{sat}}{P_{tot}-P_{sat}} \quad (P_{tot}=P_{sat}+P_a)$$

Mass fraction of air-moist mixture

$$C=\frac{\omega}{1+\omega}$$

Discussions of this paper may appear in the discussion section of a future issue. All discussions should be submitted to the Editor-in-Chief.

Manuscript Received: Oct. 17, 1998
Revision Received: Jan. 29, 1999
and Accepted: Feb. 04, 1999

水膜蒸發在充滿多孔性介質的空間中之熱質傳現象

傅武雄　柯文旺

國立交通大學機械工程研究所

摘　要

本研究以數值方法探討在一個多孔性介質中由自然對流所引發之熱、質傳現象。爲增強熱傳效率，在加熱壁面加上水膜，並且考慮潛熱和顯熱熱傳。數值方法應用 SIMPLEC 法來解 Darcy-Brinkman-Forchheimer model 的統御方程式，等熱通量、孔隙率與銅粒粒徑爲計算參數。結果顯示水膜蒸發降溫的效應明顯，在高 Darcy-Rayleigh 數，潛熱熱傳扮演降溫的重要角色。在 Darcy-Rayleigh 數小於 4 ，平均 Nusselt 數約爲 2.5；在 Darcy-Rayleigh 數介於 4 和 4469 之間，平均 Nusselt 數和 Darcy-Rayleigh 數在對數坐標中呈線性關係。

關鍵字：蒸發、多孔性介質、潛熱、顯熱。